20th IMEKO TC4 International Symposium and
18th International Workshop on ADC Modelling and Testing
Research on Electric and Electronic Measurement for the Economic Upturn
Benevento, Italy, September 15-17, 2014

Magnetic Survey of Large Magnets: a 1 to 5 scale model system

K. Buhagiar[1], Ph. Lerch[1], A. Gabard[1], M. Buzio[2], S. Sanfilippo[1], A. Foussat[3]

[1]*Paul Scherrer Institute,CH 5232 Villigen, Switzerland*
[2]*CERN, CH 1203 Geneva, Switzerland*
[3]*ITER, Saint-Paul-Lez-Durance, 13108, France*

***Abstract* – A tokamak includes large scale magnets like poloidal and toroidal field coils. Shape deformations and/or assembly errors will lead to error fields in the final configuration, which is obtained by arranging several coils of both types. In the framework of the ITER tokamak project, we are developing a magnetic measurement system capable to record, at room temperature, the current center line (CCL) of the winding pack of the toroidal superconducting field coils. The knowledge of the CCL will be compared with survey data collected during manufacturing and assembly, and possibly be used as input at the stage of assembling the TF coils in the pit of the machine. In order to validate our approach, we built a 1:5 scale TF coil single filament test platform. This contribution describes our approach and presents results obtained with this laboratory prototype.**

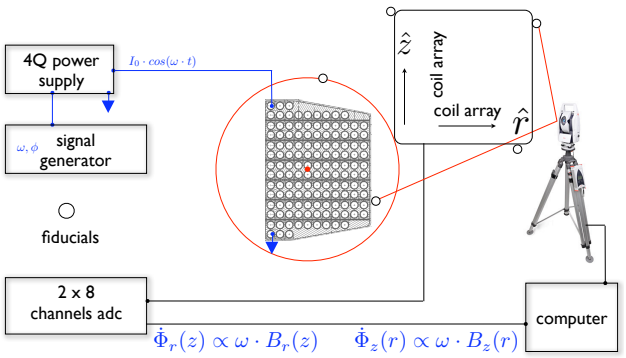

Fig. 1. Cross section of the winding pack of a TF coil (134 turns) and block diagram of the experimental set-up. The center of the 1 meter diameter circle surrounding the winding pack shows the location of the CCL.

I. INTRODUCTION

Departure from the ideal magnetic field axisymmetry in a Tokamak is caused by variations from the nominal electrical conductors configuration that produces magnetic field [1]. These deviations cause error fields and are the result of manufacturing and installation tolerances, the presence of joints and busbars, as well as the presence of ferromagnetic elements.

The current center line (CCL) of a magnet is defined as the 3D barycenter filament obtained when taking into account the spatial distribution of current (i.e cables) of the assembly. If the CCL carries the same amount of (Amp x turn) as the real object, it also produces the same long range magnetic field density profile. The detailed magnetic field modulation pattern due to the arrangement of individual cables is lost. With the knowledge of this virtual filament [2], winding geometry control can be improved. The deviations between the nominal and real CCL filaments, measured on a series of magnets can be compared to the mechanical survey data obtained along the complex manufacturing and assembly process.

ITER requires 18 toroidal field (TF) coils [3, 4, 5] which are $\approx$ 13 m x 8 m x 0.7 m objects and even larger poloidal field coils. In this context, we develop a system [6] dedicated to the magnetic determination of the CCL. A magnetic flux measurement system senses radial $B_r(P_k)$ [7] and vertical $B_z(P_k)$ field components at $k = 1$ to N locations $P_k(x, y, z)$. From the difference between the values of magnetic flux density (or gradients thereof [9]) *measured* at several locations P_k around the perimeter of the TF coil, and those *computed* at the same locations, using the nominal shape of the CCL, we wish to quantify shape deviations of the actual CCL filament. This translates into a classical inverse problem; we need to compute the magnetic field map at every P_k using an appropriate model, including a physically sound mathematical description of CCL shape changes, $\delta\mathbf{a}$. Moreover, magnetic density variation unrelated to the winding geometry, but capable to affect measurements like eddy currents, the presence of magnetic materials in the concrete floor of the premises to name just a few, must somehow be kept under control.

II. EXPERIMENTAL SET-UP

A. *Laboratory CCL at 1:5 scale*

ITER objects are large, and not at all easy to access along the complex and geographically widespread manufacturing chain. We started from the 1:1 CCL filament defined in document [8] and built a 1:5 scale single filament laboratory tool in order to validate, in practice, our approach. Two grooves were CNC-milled into a wood

ISBN-14: 978-92-990073-2-7

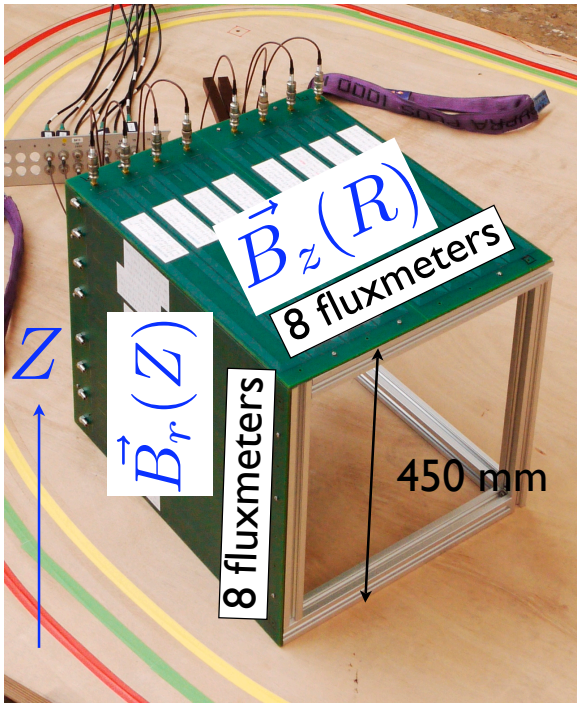

Fig. 2. Measurement system including two units of 8 spiral coils each. One coil has ≈ 4.5 m^2 of effective flux collection area and an outer size of ≈ 420 mm x 36 mm.

platform at a scale of (0.95 x 1:5) and (1.0 x 1:5). The platform is 3 m x 1.5 m in size. A one millimeter diameter Cu wire was glued into the grooves. Each turn can be electrically contacted separately. The experimental set-up is described in Ref.[6] whereas Fig. 1 shows a simplified block diagram and the cross section of the winding pack of the actual TF coil, with 134 cables. The experimental arrangement used with our 1:5 scale model is identical. A four quadrant class A amplifier driven by a signal generator is used as ac current source and is connected to the test filament. A current $I_0 \cdot cos(\omega \cdot t)$ flows through the coil and generates a time varying magnetic field $B_0 \cdot cos(\omega \cdot t + \phi)$. ω and ϕ are the circular frequency and phase shift terms, respectively. The position of the center P_k of a flux coil, expressed in the reference frame of the filament magnet under study, is determined with an optical laser tracker. We mounted two arrays of 8 pick-up coils, manufactured with PCB technology, on a cubic frame of aluminum, so as to record two orthogonal components of magnetic flux, $B_z(r, P_k)$ and $B_r(z, P_k)$. This system is shown in 2 and delivers 16 signals, to adc's. The voltage recorded at each coil is proportional to ω, and depends upon the exact shape of the current filament (Biot and Savart), the size and shape of the pick-up coils, (see Ref. [6]) as well as on the gain of the electronic acquisition chain (RC noise reduction filters and gain of the adc's require dedicated calibration steps).

B. *Data acquisition*

The analog signal from every flux meter coils is sent to a RC filter (calibrated) and further to a commercially available adc card [11]. The excitation frequency ranges between 1 and 10 Hz. The acquisition of the waveforms for each channel is adjusted (ad-hoc Labview routines) so as to record 8 full cycles and to perform a best-fit of a sine function across the data. This operation is iterated and delivers the averaged results of 30 runs. We record the amplitude of 16 induced voltages $V_r(z, P_k, \omega)$ and $V_z(r, P_k, \omega)$ which correspond to the rate of variation of magnetic flux components $\dot{\Phi}_r(z, P_k) \propto \omega \cdot B_r(z, P_k)$ and $\dot{\Phi}_z(r, P_k) \propto \omega \cdot B_z(r, P_k)$.

To survey our 1:5 scale laboratory CCL we simply move our cube on the platform, record the geodesic information at each location together with the 16 induced voltages. We record between 30 and 40 locations around the perimeter of the current filament and pay attention that the cube is always located entirely inside or outside the closed current filament.

III. PROOF OF PRINCIPLE

A. *Current filament with nominal shape*

We manufactured the groove of the 1:5 scale CCL filament using a discrete data set CCL(x_i, y_i, z_i) for the CNC mill and consider the same data set as a faithful representation of the filament in space. We use CCL(x_i, y_i, z_i) as input to compute the magnetic flux density for every location P_k at which a pick-up coil delivers a data point. Since the magnetic flux density is not constant across the entire physical area of the flux coil we segment this area in 2 x 4 subareas. Further, we use the knowledge of the orientation of the coil's principal axis and compute an array of $B_{seg}(P_k)$ values centered around P_k as well as the details of the spirals to compute the induced voltage sensed by each spiral coil $V_m(P_k)$. The subscripts $_m$ and $_e$ are used for *model* and *experimental* values, respectively. Fig. 3 shows the z-components $V_{m,z}(P_k, r)$ and $V_{e,z}(P_k, r)$, together with the relative difference $\epsilon_z = (V_{m,z} - V_{e,z})/V_{e,z}$, as function of the 8 x 41 P_k values. This grouping follows the data acquisition scheme. The first forty one points represent the complete magnetic survey around the CCL perimeter of coil 1 of the detector module. The last series of 41 points is data recorded by coil 8, which is the closest to the magnetic field source. Fig. 4 shows the corresponding radial components $V_{m,r}(P_k, z)$ and $V_{e,r}(P_k, z)$, together with the relative error ϵ_r. For radial r data, coil 1 is the closest to the source.

The only adjustable parameters allowed in the computation of the vertical and radial components of the flux variation are a global gain, very close to one, that reflects small mistakes in the evaluation of the amplitude of the excitation current. Further, we allow for global x, y and z directions shifts, which take into account small differ-

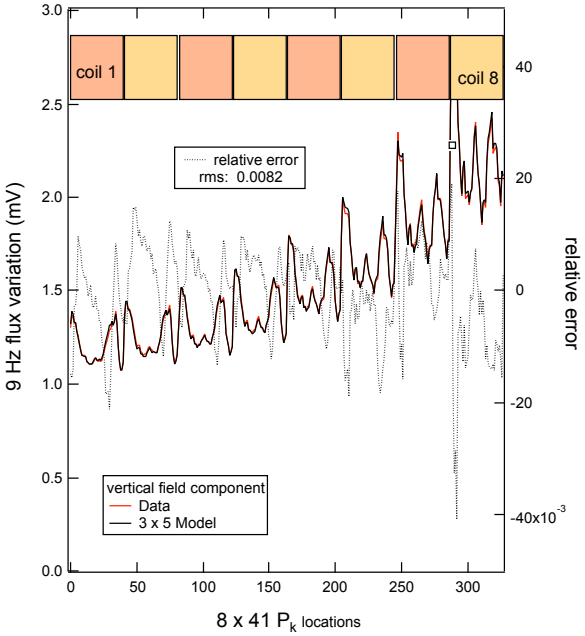

Fig. 3. Vertical component of the experimental and modeled induced voltage $V_z(P_k, r)$ values; excitation current is 6 amp, 9 Hz; 8 x 41 locations.

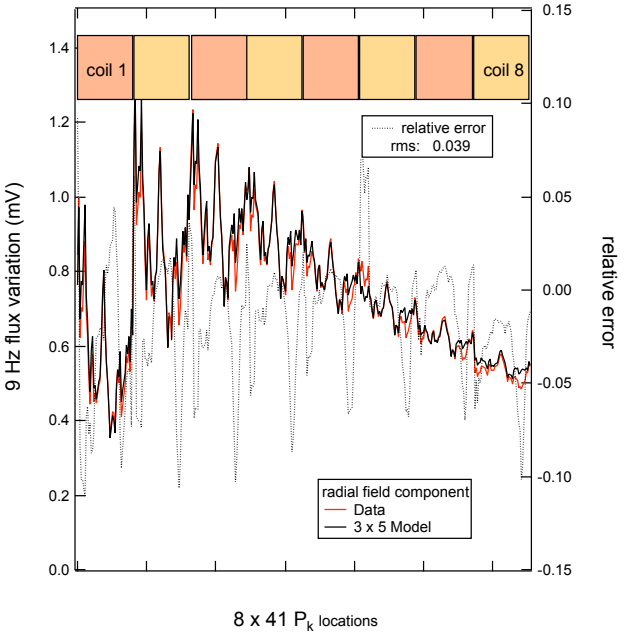

Fig. 4. Radial component [7] of the measured and computed induced voltage values $V_r(P_k, z)$; excitation current 6 amp, 9 Hz; 8 x 41 locations.

ences between the reference frame of the experiment, and the one used to mill the groove in the platform. All the other parameters used to compute the magnetic flux density and later the induced voltage are measured quantities. Although the overall agreement between experimental and computed values is good, it is striking to observe that the rms value of the relative difference in the radial component is larger than the one obtained in the z-direction.

B. *Current filament with deformed shape*

We introduce a known amount of deformation by guiding the wire into another groove over a reduced fraction of the circumference. The geodesic and magnetic survey is performed again as described above. In Fig. 5 we show a contour plot of the z-axis component of induced voltages, $V_{e,z}$ expressed in the XY fame of the 1:5 scale system, recorded with a deformed CCL. The shape (blue) of the deformed CCL is superposed onto the nominal shape (red). Each isolated dot represents a P_k point at which a induced voltage value was recorded. Very little in that plot indicates the presence of deformations. We now compute the relative differences between model and experimental values for the two known shapes of the CCL.

The polar representation shown in Fig. 6 allows to visualize the effects due to a known deformation. We estimate for each P_k the angle $\phi_k = arctg(y_k/x_k)$ and plot the absolute values of the relative error $\epsilon_z(\phi_k)$ obtained with experimental data measured on a deformed shape but computed with the nominal and deformed CCL shapes. Clearly, large deviations observed on the lowest polar plot (blue) are concentrated in the angular region where the defect was introduced. Using the CCL survey data including the actual deformation entirely cancels that large relative differences, and leaves residual errors that have a different origin. We can now envisage to introduce the term $\delta\mathbf{a}$ into the CCL and iterate the procedure, provided we are sure to observe filament shape deviations only.

This simplified approach illustrates the proof of principle and can be used to validate each steps required to acquire data, compute flux from a known filament shape, and compare model and experimental data.

IV. FACTORS AFFECTING MAGNETIC FLUX

In addition to noise, we must control the precision at which a particular measurement can be done, as well as validate the model assumptions used to compute magnetic flux. The key ingredients required to compute magnetic flux are: i) the 3D shape of the current filament that is used to estimate the magnetic flux density, ii) the precise position P_k of the center of a flux sensor and its orientation in space, iii) the details of the flux sensor, iv) the magnitude and frequency of the ac excitation current. The possible effects of eddy current flowing in large cross section metallic structures and producing a reaction magnetic field that opposes the forward field are difficult to model with accuracy. This effect has been studied in a recent experiment performed on a 1:1 scale radial plate and is described elsewhere[12]. Moreover, the presence of magnetic mate-

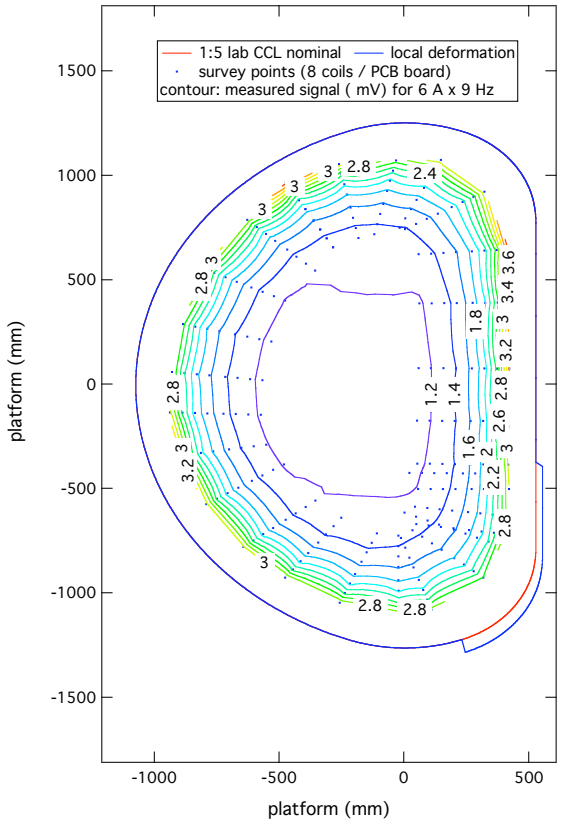

Fig. 5. Contour plot of the z-axis component of measured voltage, using a deformed filament. Each dot is a P_k point.

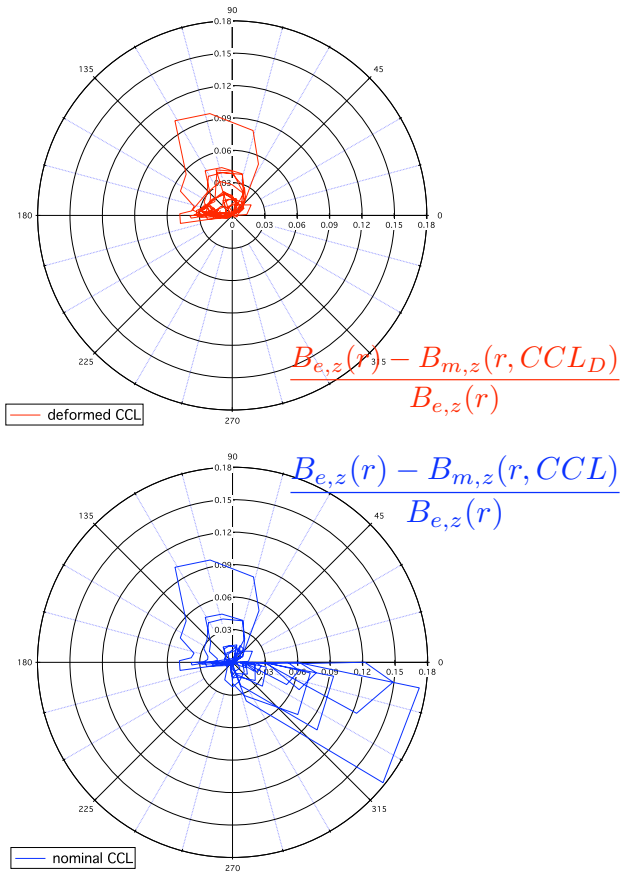

Fig. 6. Polar plots (z-axis component) of the relative difference $\epsilon_z(\phi_k)$ measured on a deformed 1:5 CCL filament. Blue: relative difference computed with the nominal CCL shape. Red: with the deformed CCL shape.

rials may introduce distortions in the magnetic field density profiles. We limit the present discussion to points i) to iii); iv) is strictly instrumental and includes noise.

A. *i) the 3D shape of the current filament*

A geometrical survey of the current filament in its groove using the optical tracker confirms that the used values for CCL(x_i, y_i) are robust. However, the z-coordinate values of the wire follow the shape of the deformed wooden platform. Thus, the CCL(z_i) values describe deviations from perfect flatness and must be taken into account. The filament reveals a clear z-axis "waviness" of 3-4 mm peak to peak, which we include into the nominal CCL(x_i, y_i) data set to obtain CCL$(x_i, y_i, z_{i,survey})$ by interpolation. A new computation using this more accurate description of the current path improves the global results only slightly.

B. *ii) the position P_k of the flux sensor*

The actual position of the center, P_k, of each sensor during a survey is not measured directly, but obtained by the determination of the position $P_c(x, y, z)$ and angular attitude in space of the detector carrier that holds the 2 units of 8 coils. P_c is measured with three optical targets firmly mounted on the holder; with the knowledge of P_c, and the attitude of the unit with respect to the reference frame used during the calibration, we apply a geodesic transformation to obtain the P_k's by using the separate calibration matrix linking P_c to each P_k on the boards. The uncertainty we obtain at P_k is 0.1 mm in all three directions.

C. *iii) the details of the flux sensor*

Each module contains 8 flux detection coils (outside dimensions 420 mm by 36 mm) fabricated with printed circuit board (PCB) technology. Each coil is formed by a precisely aligned stack of 22 rectangular, 15 turns spirals connected in series within thickness of a 3.2 mm thick board. We therefore approximate the pick-up coil as a 2D planar object. During a measurement, the sensor behaves like an analog device and integrates the flux density accurately. The equivalent computed magnetic flux collected by such a device is given by $\int\int \vec{B} \cdot d\vec{S}$. Since the magnetic flux density $B(P_k)$ produced by the 3D filament is not constant, we segment the physical area $\int\int d\vec{S}$ of the coil in n

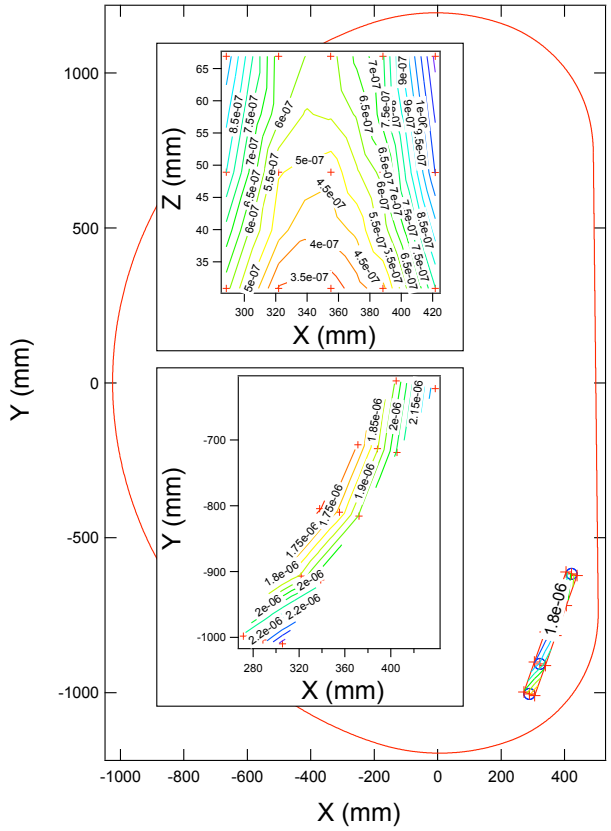

Fig. 7. XY view of the 1:5 scale laboratory model filament and one location of the two detectors. Inset top: contour plot of the radial component of magnetic flux density, computed on an array of 5 x 3 points distributed across the flux coil. Inset bottom: contour plot of the z-axis field component.

x m sub-areas in order to evaluate the integral as a discrete sum. The flux density of one sub-area is computed as the average value obtained by the flux density at each corner; total flux is obtained by summation.

The largest computation errors introduced by this simplification accumulate near curved regions of the filament, since the model assigns a constant field density value to the center of each sub-area. Fig. 7 illustrates that point for one particular location (x $\approx$ 300 mm, y $\approx$ -800 mm) of the two flux coil detectors. The two insets show the contour plots of the radial and z-axis components of magnetic flux density, computed for an array of 5 x 3 points. Improving this situation can be achieved by reducing the size of the segmentation cells, at the expense of computation time.

Fig. 8 indicates the trend taken by the relative error of the radial component $\epsilon_r(P_k)$, computed for three decreasing sizes of segmentation. The smallest segmentation unit is 68 mm x 9 mm (7x5) and requires 24 times longer computing time than a single call at one P_k without any segmentation.

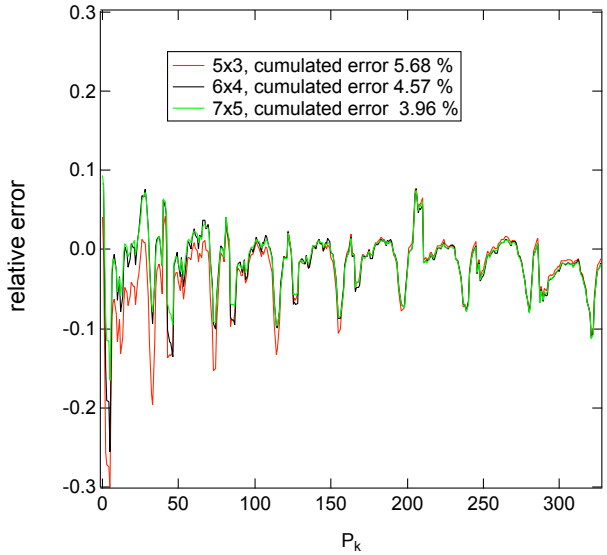

Fig. 8. Relative error of the radial component obtained with 3 different segmentations sizes.

V. CONCLUSION

A simplified 1:5 scale single filament laboratory model was built and is successfully used to validate the entire data acquisition, modeling and geodesic survey chain that shall be used to perform the magnetic survey of a 1:1 scale magnet of ITER. Eddy currents cannot be studied with this setup. However, the effect of magnetic materials, like reinforcement iron casted in the concrete floor of the measurement premises, can be studied by "scanning" a portion of hall floor with the entire platform, and comparing the results to data obtained without the effect iron. The z-axis component of magnetic flux can be modeled with an accuracy below 1%. On the other hand, the agreement obtained for the radial component is 5 times worse. We are currently investigating this effect.

For the magnetic survey of 1:1 objects, the limitation imposed by the segmentation will be less important, since the radii of curvatures will be 5 times larger. A dedicated support has been designed [10] and is presently being built.

We are currently developing an inversion algorithm, that will be used to extract shape deviations δa relative to the nominal CCL shape. The measurement strategy that is envisaged shall provide several data sets, recorded entirely inside and entirely outside the boundary of the D-shape object.

VI. AKNOWLEDGMENT

K. Buhagiar would like to thank the PSI magnet division for help during his stay as trainee. Ph. Lerch would like to thank the ATK-division members for technical help.

REFERENCES

[1] J. Knaster *et al*. "ITER non-axisymmetric error Þelds induced by its magnet system", *Fusion Engineering and Design* **86**, 1053, (2011)

[2] J. Knaster and E. Baynham, "The determination of the Current Center Line of the TF Coils of ITER", *IEEE Trans. Appl. Supercond.* **20**, 1475 (2010)

[3] F. Savary *et al*. "Status Report on the Toroidal Field Coils of the ITER Project", *IEEE Trans. Appl. Supercond.*, **20**, 381 (2010)

[4] N. Koizumi *et al*. "Development of the ITER Toroidal Field Coil Winding Pack in Japan", *IEEE Trans. Appl. Supercond.*, **20**, 385 (2010)

[5] J. Knaster *et al*. "Final assembly and installation of the ITER TF coils", *IEEE Trans. Appl. Supercond.*, **18**, 495 (2007)

[6] Ph. Lerch *et al* "Room temperature magnetic determination of the Current Center Line for the ITER TF coils", *IEEE Trans. Appl. Superc.* 23 (2013)

[7] The integration along a given CCL current path using the Biot and Savart relation gives three magnetic flux density components, B_x, B_y and B_z. We compute the radial term $B_r = (B_x^2 + B_y)^2$

[8] ITER technical drawing, ID 28HP9H, drawing 000885

[9] L. Deniau *et al*. "Magnetic Measurement of the Current Center Line of the Toroidal Field Coil of ITER at Room Temperature", *CERN-ATS-2012-048* and L. Deniau, "Magnetic Measurements of Center Current Line at Room Temperature", *IEEE Trans. Appl. Supercond.* **22**, 9001704 (2012)

[10] D. Wasmmer, Design and Construction of a Detector Support for the ITER TF Coil Magnetic Survey System, bachelor thesis in mech. ing., Technical University of Konstanz, Germany, 2014

[11] 8 channels PCI-6231 ADC card, National Instrument

[12] Ph. Lerch *et al* "Magnetic determination of the Current Center Line for the superconducting ITER TF coils", submitted